INAF
ISTITUTO NAZIONALE
DI ASTROFISICA
NATIONAL INSTITUTE
FOR ASTROPHYSICS

Publication Year	2020
Acceptance in OA	2025-03-10T15:52:58Z
Title	CHIMPS2: survey description and ¹²CO emission in the Galactic Centre
Authors	Eden, D. J., Moore, T. J. T., Currie, M. J., Rigby, A. J., Rosolowsky, E., Su, Y., Kim, Kee-Tae, Parsons, H., Morata, O., Chen, H. -R., Minamidani, T., Park, Geumsook, Ragan, S. E., Urquhart, J. S., Rani, R., Tahani, K., Billington, S. J., Deb, S., Figura, C., Fujiyoshi, T., Joncas, G., Liao, L. W., Liu, T., Ma, H., Tuan-Anh, P., Yun, Hyeong-Sik, Zhang, S., Zhu, M., Henshaw, J. D., Longmore, S. N., Kobayashi, M. I. N., Thompson, M. A., Ao, Y., Campbell-White, J., Ching, T. -C., Chung, E. J., Duarte-Cabral, A., Fich, M., Gao, Y., Graves, S. F., Jiang, X. -J., Kemper, F., Kuan, Y. -J., Kwon, W., Lee, C. W., Lee, J. -E., Liu, M., Peñaloza, C. H., Peretto, N., Phuong, N. T., Pineda, J. E., Plume, R., Puspitaningrum, E., Samal, M. R., Soam, A., Sun, Y., Tang, X. D., TRAFICANTE, Alessio, White, G. J., Yan, C. -H., Yang, A. Y., Yuan, J., Yue, N., Bemis, A., Brunt, C. M., Chen, Z., Cho, J., Clark, P. C., Cyganowski, C. J., Friberg, P., Fuller, G. A., Han, I., Hoare, M. G., Izumi, N., Kim, H. -J., Kim, J., Kim, S., Koch, E. W., Kuno, N., Lacialle, K. M., Lai, S. -P., Lee, H., Lee, Y. -H., Li, D. L., Liu, S. -Y., Mairs, S., Pan, Z., Qian, L., Scicluna, P., Shi, C. -S., Shi, H., Srinivasan, S., Tan, Q. -H., Thomas, H. S., Torii, K., Trejo, A., Umemoto, T., Violino, G., Wallström, S., Wang, B., Wu, Y., Yuan, L., Zhang, C., Zhang, M., Zhou, C., Zhou, J. J.
Publisher's version (DOI)	10.1093/mnras/staa2734
Handle	http://hdl.handle.net/20.500.12386/36623
Journal	MONTHLY NOTICES OF THE ROYAL ASTRONOMICAL SOCIETY
Volume	498

Monthly Notices of the ROYAL ASTRONOMICAL SOCIETY

MNRAS **498,** 5936–5951 (2020) doi:10.1093/mnras/staa2734
Advance Access publication 2020 September 10

CHIMPS2: survey description and ^{12}CO emission in the Galactic Centre

D. J. Eden [1★] T. J. T. Moore,[1] M. J. Currie,[2,3] A. J. Rigby [4] E. Rosolowsky [5] Y. Su,[6] Kee-Tae Kim,[7,8] H. Parsons,[2] O. Morata,[9] H.-R. Chen,[10] T. Minamidani,[11,12] Geumsook Park,[7] S. E. Ragan,[4] J. S. Urquhart,[13] R. Rani,[1] K. Tahani,[14] S. J. Billington,[13] S. Deb,[5] C. Figura,[15] T. Fujiyoshi,[16] G. Joncas,[17] L. W. Liao,[9] T. Liu,[18] H. Ma,[6] P. Tuan-Anh,[19] Hyeong-Sik Yun,[20] S. Zhang,[21] M. Zhu,[22,23] J. D. Henshaw,[24] S. N. Longmore,[1] M. I. N. Kobayashi,[25,26,27] M. A. Thompson,[28] Y. Ao,[6] J. Campbell-White,[29] T.-C. Ching,[10] E. J. Chung,[7] A. Duarte-Cabral,[4] M. Fich,[30] Y. Gao,[6,31] S. F. Graves,[2] X.-J. Jiang,[2] F. Kemper,[9,32] Y.-J. Kuan,[32,33] W. Kwon,[7,34] C. W. Lee,[7,8] J.-E. Lee,[20] M. Liu,[22] C. H. Peñaloza,[21] N. Peretto,[4] N. T. Phuong,[19] J. E. Pineda,[35] R. Plume,[36] E. Puspitaningrum,[37] M. R. Samal,[38,39] A. Soam,[7,40] Y. Sun,[6] X. D. Tang,[41] A. Traficante,[42] G. J. White,[3,43] C.-H. Yan,[32] A. Y. Yang,[44] J. Yuan,[22] N. Yue,[22] A. Bemis,[45] C. M. Brunt,[46] Z. Chen,[6] J. Cho,[47] P. C. Clark,[4] C. J. Cyganowski,[21] P. Friberg,[2] G. A. Fuller,[48] I. Han,[7,8] M. G. Hoare,[49] N. Izumi,[50] H.-J. Kim,[51] J. Kim,[7] S. Kim,[7] E. W. Koch,[5] N. Kuno,[52,53] K. M. Lacialle,[45,54] S.-P. Lai,[10,32] H. Lee,[7] Y.-H. Lee,[51] D. L. Li,[41] S.-Y. Liu,[32] S. Mairs,[2] Z. Pan,[23] L. Qian,[22] P. Scicluna,[32] C.-S. Shi,[55,56] H. Shi,[22] S. Srinivasan,[32,57] Q.-H. Tan,[6] H. S. Thomas,[58] K. Torii,[11] A. Trejo,[30] T. Umemoto,[11] G. Violino,[59] S. Wallström,[32] B. Wang,[22] Y. Wu,[60] L. Yuan,[22] C. Zhang,[60] M. Zhang,[6,24] C. Zhou[6] and J. J. Zhou[41]

Affiliations are listed at the end of the paper

Accepted 2020 September 4. Received 2020 September 4; in original form 2020 July 4

ABSTRACT

The latest generation of Galactic Plane surveys is enhancing our ability to study the effects of galactic environment upon the process of star formation. We present the first data from CO Heterodyne Inner Milky Way Plane Survey 2 (CHIMPS2). CHIMPS2 is a survey that will observe the Inner Galaxy, the Central Molecular Zone (CMZ), and a section of the Outer Galaxy in ^{12}CO, ^{13}CO, and C^{18}O ($J = 3 \rightarrow 2$) emission with the Heterodyne Array Receiver Program on the James Clerk Maxwell Telescope (JCMT). The first CHIMPS2 data presented here are a first look towards the CMZ in ^{12}CO $J = 3 \rightarrow 2$ and cover $-3^\circ \leq \ell \leq 5^\circ$ and $|\, b \,| \leq 0.^\circ5$ with angular resolution of 15 arcsec, velocity resolution of 1 km s^{-1}, and rms $\Delta\, T_A^* = 0.58$ K at these resolutions. Such high-resolution observations of the CMZ will be a valuable data set for future studies, whilst complementing the existing Galactic Plane surveys, such as SEDIGISM, the *Herschel* infrared Galactic Plane Survey, and ATLASGAL. In this paper, we discuss the survey plan, the current observations and data, as well as presenting position–position maps of the region. The position–velocity maps detect foreground spiral arms in both absorption and emission.

Key words: molecular data – surveys – stars: formation – ISM: molecules – Galaxy: centre.

1 INTRODUCTION

The formation of stars from molecular gas is the key process driving the evolution of galaxies from the early Universe to the current day. However, the regulation of the efficiency of this process (the star formation efficiency, SFE) on both the small scales of individual clouds and the larger scales of entire galaxies, is poorly understood.

In the era of ALMA, single-dish surveys play an essential role for understanding star formation in the context of Galactic environment. Advances in array detectors have enabled large surveys of the Galactic Plane to be completed in a reasonable time, producing large samples of regions for statistical analysis (e.g. Urquhart et al. 2018). By doing this, we can measure the relative impact on the SFE of Galactic-scale processes, e.g. spiral arms, or the pressure and turbulence within individual clouds.

However, untangling star formation on larger and smaller scales is complicated by the different sampling rates on these scales. Studies of extragalactic systems have produced empirical relationships, such as the Kennicutt–Schmidt (K–S) relationship (Kennicutt 1998), which scales the star formation rate (SFR) with gas density; and further relationships scaling the SFR with the quantity of dense gas ($n(\mathrm{H_2}) \geq 3 \times 10^4$ cm^{-3}; Gao & Solomon 2004; Lada et al. 2012). These correlations, though, break down on scales of 100–500 pc, a scale where the enclosed sample of molecular clouds is small (Onodera et al. 2010; Schruba et al. 2010; Kruijssen & Longmore 2014).

★ E-mail: D.J.Eden@ljmu.ac.uk

© 2020 The Author(s)
Published by Oxford University Press on behalf of the Royal Astronomical Society

Downloaded from https://academic.oup.com/mnras/article/498/4/5936/5903721 by Biblioteca Centrale - Consiglio Nazionale delle Ricerche user on 27 February 2025

Table 1. Summary of the observation parameters for the CHIMPS, COHRS, FUGIN, and SEDIGISM surveys, including CHIMPS2 for comparison.

Survey	Observed isotopologues	Transition	Longitude range	Latitude range	Angular resolution	Velocity resolution	Telescope	Reference[a]
CHIMPS	^{13}CO/C^{18}O	$J = 3 \rightarrow 2$	28–46°	$\|b\| < 0.^{\circ}5$	15 arcsec	0.5 km s^{-1}	JCMT	(1)
COHRS	^{12}CO	$J = 3 \rightarrow 2$	$10.^{\circ}25$–$55.^{\circ}25$	$\|b\| < 0.^{\circ}5$	16 arcsec	1.0 km s^{-1}	JCMT	(2)
FUGIN Inner Gal.	^{12}CO/^{13}CO/C^{18}O	$J = 1 \rightarrow 0$	10–50°	$\|b\| < 1.^{\circ}0$	20 arcsec	1.3 km s^{-1}	NRO 45-m	(3)
FUGIN Outer Gal.	^{12}CO/^{13}CO/C^{18}O	$J = 1 \rightarrow 0$	198–236°	$\|b\| < 1.^{\circ}0$	20 arcsec	1.3 km s^{-1}	NRO 45-m	(3)
SEDIGISM	^{13}CO/C^{18}O	$J = 2 \rightarrow 1$	−60–18°	$\|b\| < 0.^{\circ}5$	30 arcsec	0.25 km s^{-1}	APEX	(4)
CHIMPS2 CMZ	^{12}CO/^{13}CO/C^{18}O	$J = 3 \rightarrow 2$	−5–5°	$\|b\| < 0.^{\circ}5$	15 arcsec	1/0.5/0.5 km s^{-1}	JCMT	(5)
CHIMPS2 Inner Gal.	^{13}CO/C^{18}O	$J = 3 \rightarrow 2$	5–28°	$\|b\| < 0.^{\circ}5$	15 arcsec	0.5 km s^{-1}	JCMT	(5)
CHIMPS2 Outer Gal.	^{12}CO/^{13}CO/C^{18}O	$J = 3 \rightarrow 2$	215–225°	−2–0°	15 arcsec	1/0.5/0.5 km s^{-1}	JCMT	(5)

[a]References for survey information: (1) Rigby et al. (2016), (2) Dempsey et al. (2013), (3) Umemoto et al. (2017), (4) Schuller et al. (2017), (5) This paper.
bottom

These two apparently contradictory results are supported when the clump-formation efficiency (CFE), or dense-gas mass fraction (DGMF) within individual molecular clouds is examined. The distribution of cloud CFEs is lognormal, with values varying by two to three orders of magnitude (Eden et al. 2012, 2013); however, the CFE is fairly constant when averaged over kiloparsec scales.

The distributions of the SFEs estimated from the ratio of infrared luminosity to cloud or clump gas mass, are also found to be lognormal (Eden et al. 2015), indicating that the central-limit theorem is at play in both cases, giving a well-defined mean value when averaged over a large sample of clouds and a large area of the Galaxy. They also point to the spiral structures of the Milky Way having only a minor influence in enhancing the star formation within them (Moore et al. 2012; Urquhart et al. 2020), a conclusion also reached in M51 (Schinnerer et al. 2017). The fraction of star-forming *Herschel* sources as a function of Galactocentric radius in the Milky Way also displays no arm-associated signal (Ragan et al. 2016, 2018). Studies of other Galactic-scale mechanisms, such as shear, have found conflicting evidence for impact on the star formation (Dib et al. 2012; Suwannajak, Tan & Leroy 2014).

Despite these results, there are large-scale variations between Galactic environments that would be expected to have significant influence on the star formation process. The three major star formation stages: the conversion of atomic to molecular gas, the conversion of molecular gas to dense star-forming clumps (DGMF and CFE), then the formation of stars (SFE), all show some significant variations related to Galactocentric radius. The molecular-gas mass fraction rapidly decreases from ∼100 per cent within the inner 1 kpc to a few per cent at ∼10 kpc (Sofue & Nakanishi 2016). The DGMF peaks at 3–4 kpc, and drops within the Galactic Centre, where the disc may become stable against large-scale gravitational collapse (Kruijssen et al. 2014), whilst the SFE also drops dramatically in the central 0.5 kpc when compared to the dense gas (Longmore et al. 2013; Urquhart et al. 2013). These reductions are within the region swept by the bar where, in external galaxies, the SFR is suppressed for the life of the bar (James & Percival 2016, 2018). However, when compared to the total gas mass, the SFE is consistent with the K–S relationship (Yusef-Zadeh et al. 2009; Sormani et al. 2020).

The physics of molecular clouds are important in regulating star formation, since triggering and local environment are only thought to cause 14–30 per cent of star formation (Kendrew et al. 2012; Thompson et al. 2012). There is some evidence that the clouds in the Central Molecular Zone (CMZ) exhibit low SFE as they are subject to mainly solenoidal turbulence (Federrath et al. 2016), as opposed to the compressive turbulence found in spiral-arm clouds. Therefore, to examine the internal physics, high-resolution observations of large samples of molecular clouds are required in different transitions and isotopologues such as the ^{13}CO/C^{18}O ($J = 3 \rightarrow 2$) Heterodyne Inner Milky Way Plane Survey (CHIMPS; Rigby et al. 2016), the CO High-Resolution Survey (COHRS; Dempsey, Thomas & Currie 2013), the FOREST Unbiased Galactic-plane Imaging survey with the Nobeyama 45-m telescope (FUGIN; Umemoto et al. 2017), and the Structure, Excitation, and Dynamics of the Inner Galactic Interstellar Medium survey (SEDIGISM; Schuller et al. 2017).

CHIMPS (Rigby et al. 2016) was a survey covering approximately 18 deg^2 of the northern inner Galactic Plane. The survey was conducted with the Heterodyne Array Receiver Program (HARP; Buckle et al. 2009) upon the James Clerk Maxwell Telescope (JCMT) in the $J = 3 \rightarrow 2$ rotational transitions of the CO isotopologues ^{13}CO and C^{18}O, which have frequencies of 330.587 and 329.331 GHz, respectively. The CHIMPS survey covered longitudes of $\ell = 28$–46° at latitudes of $|b| < 0.^{\circ}50$.

COHRS (Dempsey et al. 2013) was also a JCMT-HARP survey of the inner Galactic Plane but in the $J = 3 \rightarrow 2$ rotational transition of ^{12}CO at a frequency of 345.786 GHz. The longitude range of the initial release covers $\ell = 10.^{\circ}25$–$55.^{\circ}25$, with varying latitudes between $|b| < 0.^{\circ}50$ and $|b| < 0.^{\circ}25$. Full coverage details and a survey description can be found in Dempsey et al. (2013).

FUGIN (Umemoto et al. 2017) observed the inner Galaxy ($\ell = 10$–50°, $|b| < 1.^{\circ}0$) and a portion of the Outer Galaxy ($\ell = 198$–236°, $|b| < 1.^{\circ}0$) using the FOREST receiver (Minamidani et al. 2016) upon the Nobeyama 45-m telescope in the $J = 1 \rightarrow 0$ transition of the three isotopologues, ^{12}CO, ^{13}CO, and C^{18}O. The FUGIN survey is at an approximate resolution of 15 arcsec, matching the CHIMPS and COHRS surveys, allowing for column density and temperatures to be calculated from a local thermodynamic equilibrium (LTE) approximation (Rigby et al. 2019).

SEDIGISM (Schuller et al. 2017) completes the isotopologue range of CO surveys by observing ^{13}CO and C^{18}O in the $J = 2 \rightarrow 1$ rotational transition. SEDIGISM is observed at the APEX telescope at a resolution of 30 arcsec. The longitude range is $-60^{\circ} \leq \ell \leq 18^{\circ}$, and latitude range is $|b| < 0.^{\circ}50$.

The coverage of the CHIMPS, COHRS, FUGIN, and SEDIGISM surveys are summarized in Table 1, along with the CHIMPS2 survey regions introduced in this paper.

In this paper, we describe the CHIMPS2 survey and present the first data resulting from it, being the ^{12}CO $J = 3 \rightarrow 2$ emission from the CMZ. The structure of this paper is as follows: Section 2 introduces the CHIMPS2 survey, the observing strategy and science goals. Section 3 describes the data and the data reduction, whilst Section 4 introduces the intensity maps from the ^{12}CO CMZ portion of the CHIMPS2 survey, and Section 5 provides a summary.

Downloaded from https://academic.oup.com/mnras/article/498/4/5936/5903721 by Biblioteca Centrale - Consiglio Nazionale delle Ricerche user on 27 February 2025

Table 2. The time awarded to the CHIMPS2 project within each JCMT weather band, and the corresponding sky opacity.

Weather band	Hours awarded	Sky Opacity τ_{225}	CO isotopologue
1	85.5	<0.05	^{13}CO and C^{18}O
2	218.4	0.05–0.08	^{13}CO and C^{18}O
4	50.0	0.12–0.20	^{12}CO
5	50.0	>0.20	^{12}CO

2 CHIMPS2

CHIMPS2 is the follow-up to the CHIMPS and COHRS surveys and is a Large Program on the JCMT.[1] The project was awarded 404 h across four of the five JCMT weather bands to observe parts of the Inner and Outer Galaxy and the CMZ in the $J = 3 \rightarrow 2$ transition of ^{12}CO, ^{13}CO, and C^{18}O. Table 2 summarizes the number of hours awarded in each band. Weather Bands 1 and 2 are required for the ^{13}CO and C^{18}O observations, since these transitions sit on the shoulder of the 325-GHz atmospheric water-vapour absorption feature, while Bands 4 and 5 are utilized for the ^{12}CO data. Observations began in 2017 June and are still ongoing.

2.1 Observing strategy

The CHIMPS2 survey contains three components, the Inner and Outer Galaxy and the CMZ, with slightly differing observing strategies employed in each portion. The general observing strategy is to follow that of CHIMPS for ^{13}CO and C^{18}O and COHRS for the ^{12}CO observations. Full details can be found in Rigby et al. (2016) and Dempsey et al. (2013); however, a brief description is included here, for completeness.

Following the CHIMPS strategy, CHIMPS2 is constructed of a grid of individual tiles orientated along Galactic coordinates. Tiles are 21 × 21 arcmin in size spaced 20 arcmin apart, so that a 3 × 3 set of nine tiles covers an area of ∼1 deg^2. The overlap allows for calibration adjustments between tiles and correction of edge effects. The data have native angular resolution of 15 arcsec. The ^{13}CO and C^{18}O ($J = 3 \rightarrow 2$) lines are observed simultaneously with a 250-MHz frequency bandwidth, giving a native velocity resolution of 0.055 km s^{-1}. These data are binned to 0.5 km s^{-1}, covering the $V_{\rm LSR}$ velocity ranges of −50 to 150 and −75 to 125 km s^{-1}, depending on the longitude of the observations. The data have antenna-temperature sensitivities of 0.58 and 0.73 K in ^{13}CO and C^{18}O, corresponding to H_2 column densities of 3×10^{20} and 4×10^{21} cm^{-2}, assuming a typical excitation temperature of 10 K (e.g. Rigby et al. 2019).

The COHRS data were observed in tiles up to 0.°5 × 0.°5 at a spatial resolution of 13.8 arcsec and a raw spectral resolution of 0.42 km s^{-1} in the velocity range −230 to 355 km s^{-1}. The data were binned spectrally to a resolution of 0.635 km s^{-1}. Taken across multiple weather bands, the sensitivity at this resolution is ∼0.3 K (Park et al., in preparation). Since the original paper (Dempsey et al. 2013), new observations have been taken to complete a uniform latitude range of $|b| < 0.°50$, to extend the longitude coverage to $\ell = 9.°50$–$62.°25$, and to re-observe the noisiest tiles (Park et al., in preparation).

The Inner Galaxy portion of the CHIMPS2 survey is an extension of the CHIMPS and COHRS projects into the inner 3 kpc of the Milky Way. This will extend these surveys to longitudes of $\ell = 5°$ between latitudes of $|b| < 0.°50$ from their current longitude limits of $\ell = 28°$ and $\ell = 10°$ for CHIMPS and COHRS, respectively. The observing strategy in this region matches that of the CHIMPS and COHRS surveys, although the ^{12}CO tiles observed in CHIMPS2 will match the 21 × 21 arcmin tiles of CHIMPS.

The Outer Galaxy segment of CHIMPS2 covers the longitude and latitude ranges $215° \leq \ell \leq 225°$, $-2° \leq b \leq 0°$, a section partly covered by the FUGIN survey and entirely by the *Herschel* infrared Galactic Plane Survey (Hi-GAL; Molinari et al. 2010a, b), where over 1000 star-forming and pre-stellar clumps were identified (Elia et al. 2013). This regions is also entirely covered by the Forgotten Quadrant Survey in ^{12}CO and ^{12}CO $J = 1 \rightarrow 0$ (Benedettini et al. 2020). The ^{12}CO emission is, however, quite sparse in this area of the Galaxy, and a corresponding blind survey of ^{13}CO and C^{18}O would result in many empty observing tiles. Therefore, using the relationship of ^{13}CO brightness temperature from CHIMPS (Rigby et al. 2016) to that of ^{12}CO from COHRS, as displayed in the left-hand panel of Fig. 1, we are able to select regions that require ^{13}CO and C^{18}O follow-up. The threshold for this was determined to be at a ^{12}CO brightness temperature of 5 K.

The final segment of CHIMPS2 covers the CMZ between longitudes of $\ell = \pm 5°$ in the latitude range of $|b| < 0.°50$. This range covers the 850-μm continuum emission presented in Parsons et al. (2018). The extended velocity range of ∼550 km s^{-1} present in the CO emission from the Galactic Centre (Dame, Hartmann & Thaddeus 2001), requires the use of the 1-GHz bandwidth mode of HARP. In this mode, ^{13}CO and C^{18}O cannot be observed simultaneously. Therefore, the ^{13}CO is observed as a blind survey, while C^{18}O data are taken as follow-up observations towards areas determined from the brightness-temperature relationship from CHIMPS (Rigby et al. 2016), displayed in the right-hand panel of Fig. 1. A ^{13}CO brightness-temperature threshold of 3 K was adopted.

The longitude coverage of the CHIMPS, CHIMPS2, and COHRS surveys are shown in Fig. 2. The FUGIN and SEDIGISM surveys are included due to the complementary nature of their observations. The CHIMPS2 latitude coverage in the Outer Galaxy follows that of Hi-GAL (Molinari et al. 2016) and is shown in Fig. 3, where the FUGIN survey latitude range is also displayed.

2.2 Science goals

The science goals of the CHIMPS2 project are multifaceted, and intended to give us a greater understanding of the effect of environment on the star formation process. The main goals are outlined below.

(i) Production of comparative samples of Galactic molecular clouds across a range of Galactic environments with cloud properties, analysed using complementary CO $J = 1 \rightarrow 0$ surveys such as FUGIN (Umemoto et al. 2017) and Milky Way Imaging Scroll Painting (MWISP; Gong et al. 2016; Su et al. 2019). Line-intensity ratios are found to be robust indicators of excitation conditions (e.g. Nishimura et al. 2015), with simulations validating these methods (Szűcs, Glover & Klessen 2014). Multitransition models simulating observations, such as those of Peñaloza et al. (2017), Peñaloza et al. (2018), will refine current LTE approximate methods (Rigby et al. 2019).

(ii) Combine with Hi-GAL (Molinari et al. 2016; Elia et al. 2017), JCMT Plane Survey (JPS; Moore et al. 2015; Eden et al. 2017), ATLASGAL (Contreras et al. 2013; Urquhart et al. 2014), and other continuum data to map the SFE and DGMF in molecular gas and constrain the mechanisms chiefly responsible for the regulation of SFE. The dense-gas SFE is largely invariant on ∼kpc scales in the Inner Galaxy disc (Moore et al. 2012; Eden et al. 2015) but falls significantly within the central 0.5 kpc (Longmore et al. 2013; Urquhart

[1] https://www.eaobservatory.org/jcmt/science/large-programs

Downloaded from https://academic.oup.com/mnras/article/498/4/5936/5903721 by Biblioteca Centrale - Consiglio Nazionale delle Ricerche user on 27 February 2025

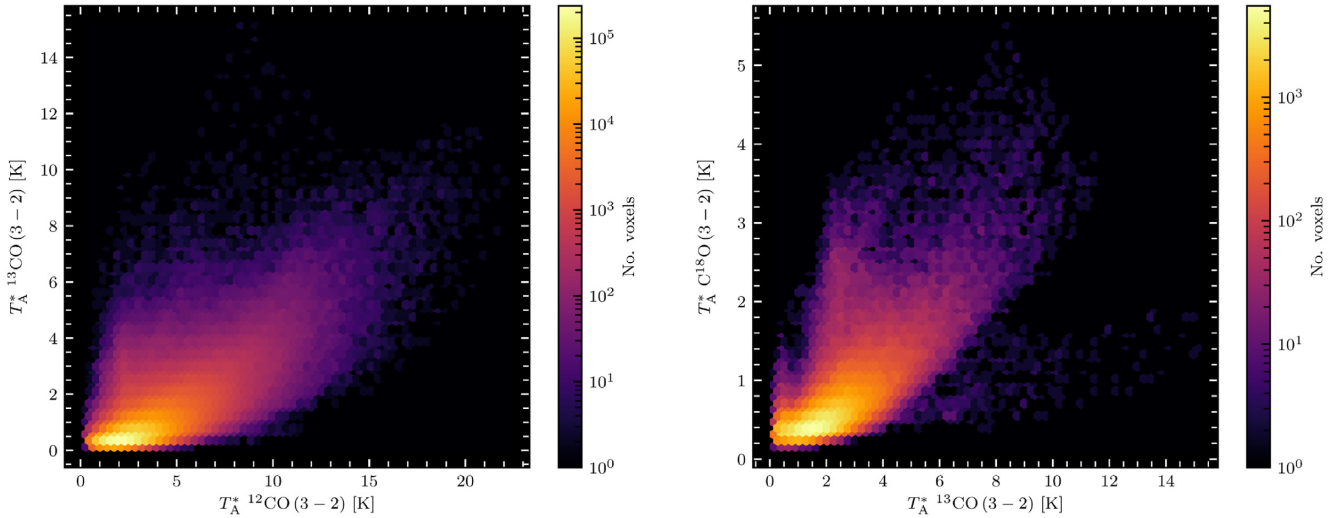

Figure 1. Comparisons of brightness temperatures used to determine observing thresholds for CHIMPS2. Left-hand panel: ^{12}CO and ^{13}CO $J = 3 \rightarrow 2$ from COHRS and CHIMPS, respectively, used to select the detection threshold of ^{13}CO for the Outer Galaxy segment. Right-hand panel: ^{13}CO and C^{18}O from CHIMPS used to select the detection threshold of C^{18}O for the CMZ segment.

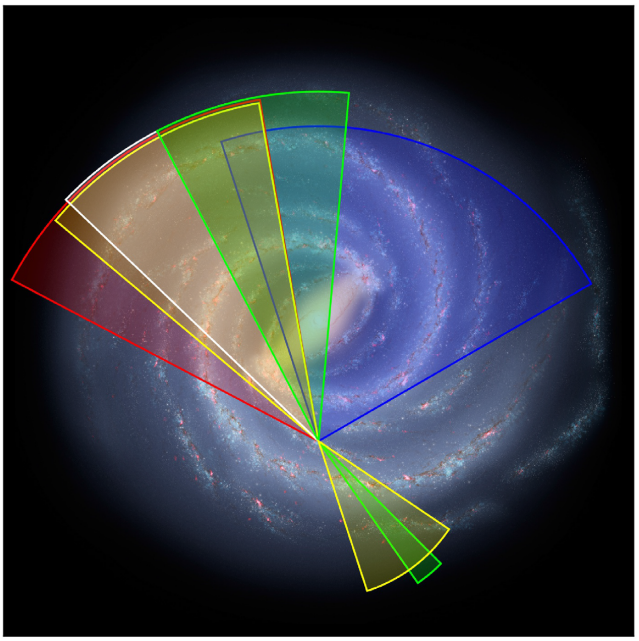

Figure 2. The area of the Galaxy covered by the CHIMPS2 survey (green segments). Complementary surveys are shown for comparison of their longitude coverage, COHRS (red), CHIMPS (white), yellow (FUGIN), and SEDIGISM (blue). The background image is the artist's impression of the Milky Way by Robert Hurt of the Spitzer Science Center, made in collaboration with Robert Benjamin.

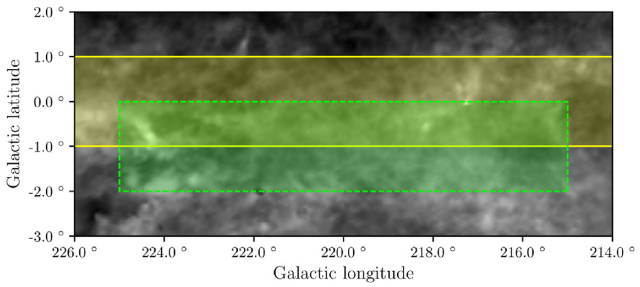

Figure 3. The area of the Outer Galaxy covered by CHIMPS2 (green dashed) and FUGIN (yellow). FUGIN is extended to longitudes of $\ell = 198^\circ$ to $\ell = 236^\circ$. Hi-GAL covers the same area as CHIMPS2. The background image is the *Planck* dust opacity map (Planck Collaboration XI 2014).

et al. 2013). Comparing these regions, along with the Outer Galaxy, where the metallicity is much lower (Smartt & Rolleston 1997), and the bar-swept radii will increase our understanding of the impact of environment on the star formation process. Variations within the CMZ may also provide insight into high-redshift star formation, since the physical condition of the clouds in this region are similar to those in galaxies at $z \sim 2$–3 (Kruijssen & Longmore 2013).

(iii) Analyse the turbulence within molecular clouds and its relationship to the large variations in SFE and DGMF/CFE between one cloud and another (Eden et al. 2012, 2013, 2015). The ratio of compressive to solenoidal turbulence in molecular clouds to the CFE and SFE may determine how the internal physics of molecular clouds is altering the star formation (Brunt & Federrath 2014; Federrath et al. 2016; Orkisz et al. 2017).

(iv) Determine Galactic structure as traced by molecular gas and star formation, and the relationship between the two. The CHIMPS survey found significant, coherent, inter-arm emission (Rigby et al. 2016), identified as a connecting spur (Stark & Lee 2006) of the type identified in external systems (e.g. Elmegreen 1980).

(v) Use comparable neutral-hydrogen data (e.g. THOR; Beuther et al. 2016) to constrain cloud-formation models and relate turbulent conditions within molecular clouds to those in the surrounding neutral gas. The first stage of the macro star formation process is the conversion of neutral gas into molecular gas and therefore clouds (Wang et al. 2020). The comparison of the THOR survey with CHIMPS2 data will allow estimates of the efficiency of this process, as well as the underlying formation process (e.g. Bialy et al. 2017) to be made.

(vi) Study the relationship of filaments to star formation, and of gas flow within filaments to accretion and mass accumulation in cores and clumps. The filaments in question cover different scales. Several long (>50 pc) filamentary structures have been identified

Downloaded from https://academic.oup.com/mnras/article/498/4/5936/5903721 by Biblioteca Centrale - Consiglio Nazionale delle Ricerche user on 27 February 2025

Table 3. The off positions for the CMZ observations in the CHIMPS2 survey.

Galactic longitude (°)	Galactic latitude (°)
−2.50	2.50
0.78	−2.75
2.60	−2.50
3.00	−2.50
5.00	2.50

(Ragan et al. 2014; Zucker, Battersby & Goodman 2015), and the CHIMPS2 data will allow for a determination of how much molecular gas is contained within these structures. On smaller scales, *Herschel* observations have shown a web of filamentary structures (e.g. André et al. 2010; Schisano et al. 2014) in which star-forming clumps are hosted (Molinari et al. 2010b). The gas flow into these clumps can be traced by the high-resolution CHIMPS2 data (e.g. Liu et al. 2018).

(vii) Test current models of the gas kinematics and stability in the Galactic-centre region, the flow of gas from the disc, through the inner 3-kpc region swept by the Galactic Bar and into the CMZ. Models of the gas flows into the centres of galaxies give signatures of these flows (e.g Krumholz, Kruijssen & Crocker 2017; Armillotta et al. 2019; Sormani et al. 2019; Tress et al. 2020), and the CHIMPS2 data can determine the mass-flow rate, the nature of the flows and the star-forming properties of these clouds.

3 DATA AND DATA REDUCTION

The data reduction for the ^{12}CO component of the CHIMPS2 survey broadly followed the approach used for COHRS (Dempsey et al. 2013), namely using the REDUCE_SCIENCE_NARROWLINE recipe of the ORAC-DR automated pipeline (Jenness & Economou 2015), and employing the techniques described by Jenness et al. (2015). The pipeline invoked the Starlink applications software (Currie et al. 2014), including ORAC-DR, from its 2018A release. However, some new or improved ORAC-DR code was developed to address specific survey needs.

Since the original COHRS reductions were completed, many improvements have been made to the reduction recipe, yielding better-quality products. These include automated removal of emission from the reference (off-position) spectrum that appear as absorption lines in the reduced spectra and can bias baseline subtraction, flat-fielding using a variant of the Curtis, Richer & Buckle (2010) summation method, and masking of spectra affected by ringing in Receptor H07 (Jenness et al. 2015).

The reduced spectral (position, position, velocity) cubes were re-gridded to 6-arcsec spatial pixels, convolved with a 9-arcsec Gaussian beam, resulting in 16.6-arcsec resolution. This produces an improvement on existing ^{12}CO ($J = 3 \rightarrow 2$) data (e.g. Oka et al. 2012). Cubes with both the 'native' spectral resolution and $\Delta V = 1\,\mathrm{km\,s^{-1}}$ were generated. The cleaning came first because it included the identification and masking of spectra that contained some extraneous signal comprising alternate bright and dark spectral channels. A first-order polynomial was used to fit the baselines (aligning with COHRS; Dempsey et al. 2013), although in the CMZ half of the baselines did require fourth-order polynomials.

The reduction of each map was made twice. The first pass used fully automated emission detection and baseline fitting, or adopted the recipe parameters of an abutting reduced tile. A visual inspection of the resultant spectral cube, tuning through the velocities and plotting the tile's integrated spectrum, enabled refined baseline and flat-field velocity range recipe parameters to be set. Also, any residual non-astronomical artefacts from the raw time series not removed in the quality-assurance phase of the reductions, and contamination from the off-position spectrum were assessed. In some cases of the former, such as transient narrow spikes, these were masked in the raw

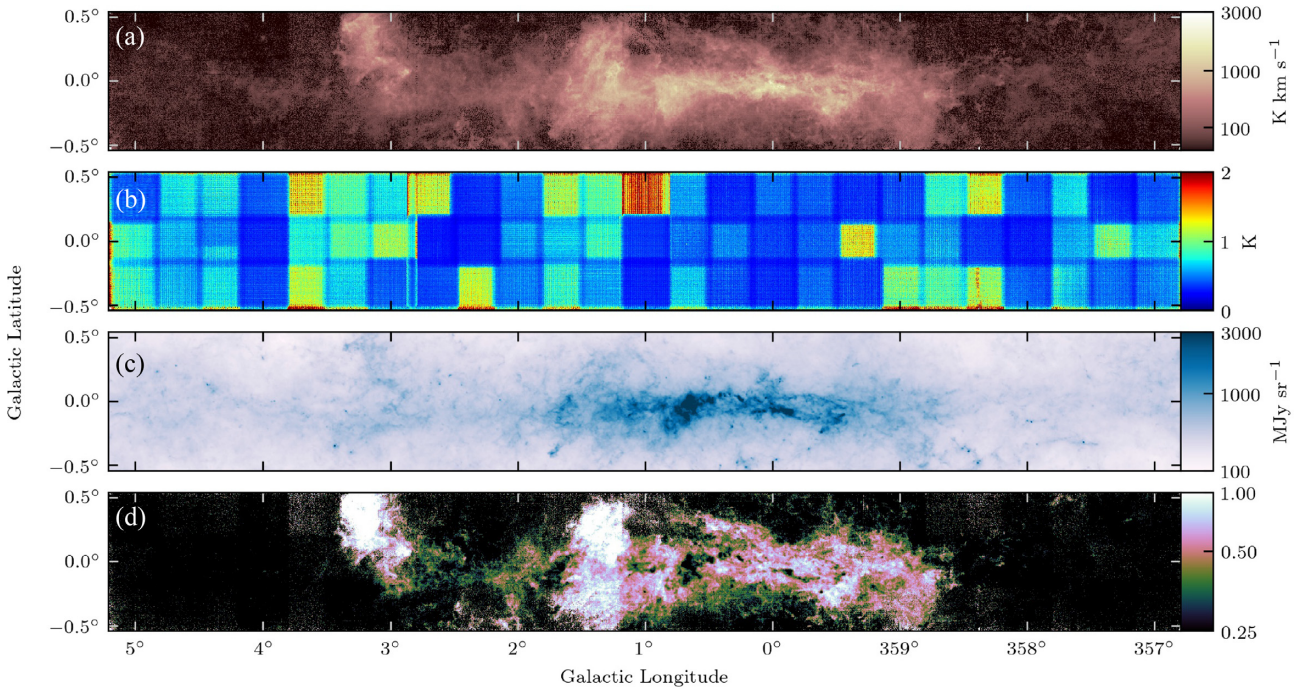

Figure 4. (a) The integrated emission from the ^{12}CO $J = 3 \rightarrow 2$ CMZ data obtained as of 2018 October. Each spectrum was integrated over all velocity channels; (b) variance map of the ^{12}CO $J = 3 \rightarrow 2$ CMZ data displayed in (a); (c) *Herschel* 500-μm surface brightness distribution from the Hi-GAL survey (Molinari et al. 2016); (d) CMZ ratio of ^{12}CO $J = 3 \rightarrow 2$ integrated intensity (a) to *Herschel* Hi-GAL 500-μm surface brightness (c).

Downloaded from https://academic.oup.com/mnras/article/498/4/5936/5903721 by Biblioteca Centrale - Consiglio Nazionale delle Ricerche user on 27 February 2025

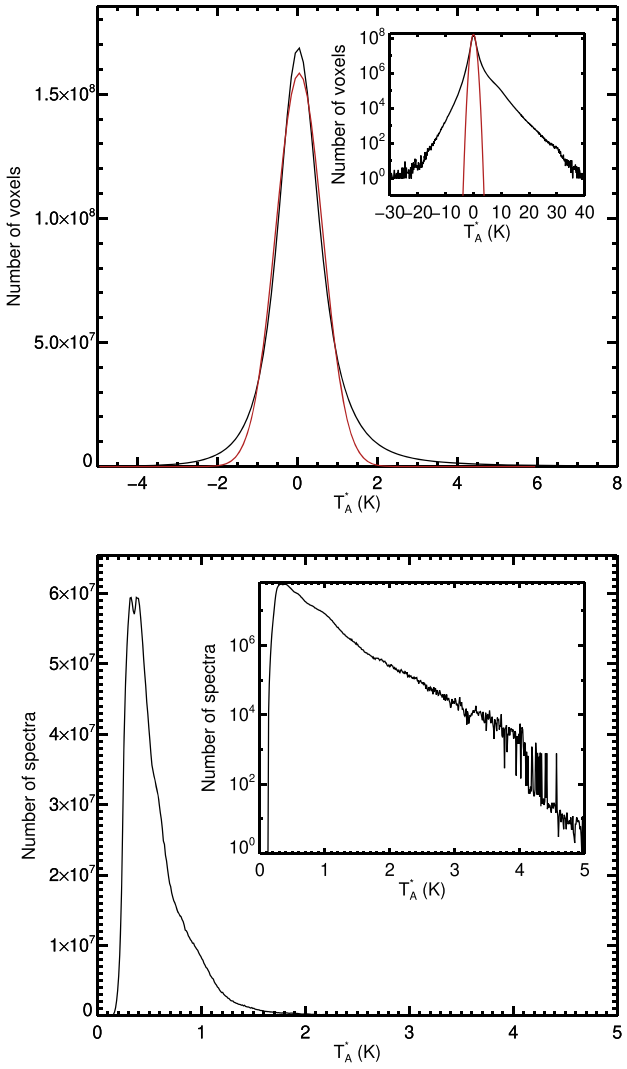

Figure 5. Top panel: Histogram of all voxels in Panel (a) of Fig. 4. The red lines display the result of a Gaussian fit to the distribution. The inset shows the distribution and Gaussian fit on a logarithmic scale. Bottom panel: Histogram of the noise values in Panel (b) of Fig. 4. The double bump is due to the differing observing conditions across the map, as seen in Dempsey et al. (2013). The inset shows the same distribution on a logarithmic scale.

data before the second reduction. Approximately 7 per cent of the tiles exhibited reference emission, which was removed by ORAC-DR using an algorithm that will be described in a forthcoming paper on the COHRS Second Release (Park et al., in preparation). The off-positions employed in the CHIMPS2 CMZ data are listed in Table 3.

Only 2 of 75 ^{12}CO CMZ tiles could not be flat fielded. In the best-determined flat-fields, the corrections were typically less than 3 per cent, although receptor H11 was circa 8 per cent weaker than the reference receptor. Example sets of recipe parameters are given in Appendix A.

All intensities given in this paper are on the T_A^* scale. To convert this to the main-beam temperature scale, $T_{\rm nmb}$, use the following relation $T_{\rm mb} = T_A^*/\eta_{\rm mb}$, where $\eta_{\rm mb}$ is the main detector efficiency and has a value of 0.72 (Buckle et al. 2009).

4 RESULTS: ^{12}CO IN THE CMZ

We are presenting the first results from the CHIMPS2 survey. These are the ^{12}CO $J = 3 \rightarrow 2$ emission within the CMZ. They provide a first look at the potential science that can be achieved with such data, which have greater resolution and/or trace higher densities than other large-scale CO surveys of the CMZ across the transition ladder ($J = 1 \rightarrow 0$; Bally et al. 1987; Oka et al. 1998; Dame et al. 2001; Barnes et al. 2015; $J = 2 \rightarrow 1$; Schuller et al. 2017; $J = 3 \rightarrow 2$; Oka et al. 2012). The data will be combined with the corresponding CHIMPS2 ^{13}CO $J = 3 \rightarrow 2$ results in a future release, along with a kinematic and dynamic analysis of the CO-traced molecular gas in the CMZ.

4.1 Intensity distribution

Panel (a) of Fig. 4 shows the map of integrated intensity of ^{12}CO $J = 3 \rightarrow 2$ in the CMZ region between $\ell = 357^\circ$ and $\ell = +5^\circ$, $|b| \leq 0.^\circ5$, constructed from data obtained up to the end of 2018. Panel (b) of Fig. 4 shows the ^{12}CO $J = 3 \rightarrow 2$ intensity variance array mosaic and hence the relative noise levels in each constituent tile within the CMZ survey region.

A histogram of the voxel values of the map in Panel (a) of Fig. 4 is displayed in the top panel of Fig. 5. The distribution is modelled by a Gaussian function with a mean of 0.05 K and a standard deviation of 0.58 K. The data distribution departs from the Gaussian in the negative wing due to non-Gaussian noise and non-uniform noise across the data set. In the positive wing, the excess comes from the real emission and the aforementioned noise. A histogram of the rms noise values from the variance maps in Panel (b) of Fig. 4 are displayed in the bottom panel of Fig. 5. Each pixel in these variance maps represents one complete spectrum from the data cube. The values in the histogram are the square root of those in the map, giving the standard deviation. The distribution peaks at 0.38 K, comparable with the value obtained from the Gaussian fit in the emission in the top panel of Fig. 5.

500-μm continuum-emission data from the *Herschel* Hi-GAL project (Molinari et al. 2010a, 2011b) at 37-arcsec resolution are displayed in Panel (c) of Fig. 4. Panel (d) of Fig. 4 shows the distribution of the ratio of ^{12}CO $J = 3 \rightarrow 2$ integrated intensity to 500-μm continuum surface brightness. The ratio values (while arbitrary) range from ∼0.1 to 2.0 – a factor of ∼20.

Figs 6 and 7 show the ^{12}CO $J = 3 \rightarrow 2$ emission integrated over 50-km s^{-1} velocity windows within the range −250 to 300 km s^{-1}, with no emission detected at velocities lower than −250 km s^{-1}.

Fig. 8 is the same as Panel (d) in Fig. 4 but with the longitude range limited to $\ell = -1^\circ$ to $1.^\circ7$. A number of compact minima coincident with bright regions in both the continuum and CO-line maps can be seen by eye and appear to represent high column-density objects in which the CO emission is reduced due to, e.g. high optical depth. In order to produce an objective list of these sources, we applied the CUTEX object-detection package (Molinari et al. 2011a, 2017) to the inverted (reciprocal) ratio image. CUTEX was chosen as it was designed to deal with extended backgrounds in *Herschel* data. The detection thresholds were four times the rms noise in the second derivative (curvature) data and a minimum of four contiguous pixels. The resulting sample was then filtered to remove sources smaller than 35 arcsec in either axis, to represent the 500-μm *Herschel* beam size. The detected sources are marked in Fig. 8 as cyan squares and listed in Table 4.

As can be seen, not all the visible compact minima were detected by CUTEX, including several well-known sources. Table 4 lists several

Downloaded from https://academic.oup.com/mnras/article/498/4/5936/5903721 by Biblioteca Centrale - Consiglio Nazionale delle Ricerche user on 27 February 2025